Microelectronic Engineering 86 (2009) 99–105

Contents lists available at ScienceDirect

Microelectronic Engineering

journal homepage: www.elsevier.com/locate/mee

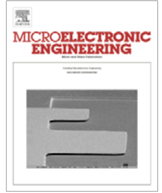

Reflectivity degradation of grazing-incident EUV mirrors by EUV exposure and carbon contamination

H. Shin *, J.R. Sporre, R. Raju, D.N. Ruzic

Center for Plasma Material Interactions, Department of Nuclear, Plasma and Radiological Engineering, University of Illinois at Urbana-Champaign, 104 S. Wright Street, Urbana, IL 61801, USA

ARTICLE INFO

Article history:
Received 13 August 2008
Accepted 13 October 2008
Available online 1 November 2008

Keywords:
Carbon contamination
Sputtering
Reflectivity
EUV mirrors
Photoelectron

ABSTRACT

Reflectivity degradation of grazing-incident extreme ultraviolet (EUV) mirror samples by EUV exposure was investigated in a commercial XTS 13-35 EUV source. The roughness of EUV exposed samples increases with an increase in exposure time due to the erosion of sample surface by ions and neutrals, or deposition of contaminant such as carbon on the sample surface. While energetic debris certainly affects mirror reflectivity, the loss in reflectivity observed in EUV exposed samples surpassed that which would be attributable simply to induced surface roughness through sputtering. Surface analysis of the EUV mirror sample surface after exposure confirmed that carbon contamination was present. Experimentally measured reflectivity of EUV mirrors showed degradation after EUV exposure due to the carbon contamination present in the investigated system. The measured reflectivity data were fitted by changing the carbon film thickness using a bi-layer mirror model in the CXRO simulator. The experimentally measured values of reflectivity are in good agreement with the simulation results. The contamination rate was found to be dependent on the carbon contamination thickness. The contamination rate is fast (7×10^{-5} nm/shot) in the beginning of contamination growth whereas it gets slower (2×10^{-5} nm/shot) as carbon builds up on the Ru mirror surface. An analytical model taking the sputtering by ions into account was developed to understand the variation of carbon contaminant deposition rate with exposure time. In our model, the fast contamination rate in the beginning of carbon buildup is explained by the interplay of photo electron emission and the varying sputtering yield of the growing carbon layer on the EUV mirror.

© 2008 Elsevier B.V. All rights reserved.

1. Introduction

Extreme ultraviolet lithography (EUVL), the next generation lithography technique that will be used for patterning features less than 22 nm, has been progressing remarkably quickly in the face of the underlying technical issues that have made EUVL integration impossible in the past. These technical issues include the ability to create a high power EUV source, the maintenance of EUV mirrors through the use of debris mitigation and the cleaning of contaminants in order to allow long lifetime, the development of photo resist with low line edge roughness (LER), as well as the development of defect-free EUV mask. Each challenge needs to be overcome for EUVL to be viable for high volume manufacturing (HVM). Nevertheless, EUV mirror reflectivity degradation, due to contamination within the EUV source, is of greater concern because it directly affects source power at intermediate focus (IF) and therefore directly affects the cost of ownership (CoO). Therefore, it is important to understand what affects reflectivity of EUV mirrors in the EUV source system. Several groups have reported EUV reflectivity degradation by ion debris buildup or erosion [1–3], carbon contamination [4], and oxidation [5]. Some cleaning methods for each type of contamination were proposed. In an EUV source using high-conversion-efficient Sn fuel, debris buildup can be cleaned by atomic hydrogen cleaning [6] or plasma etching [7]. Carbon contamination can also be removed by atomic hydrogen [6] or molecular oxygen [8]. Oxidation is known as irreversible contamination since it alters the surface layer but can be mitigated by ethanol [9] or carbon monoxide exposure under electron irradiation [10].

In this study, the effect of exposure time on the reflectivity degradation of grazing-incident EUV mirror is investigated. Changes in EUV reflectivity are measured on the samples exposed in a discharge produced plasma (DPP) EUV source chamber for varying durations. By interpreting the measured reflectivity, we supplement a mechanism of carbon contamination in EUV source system, where energetic ions are present as well as photons. The mechanism of carbon contamination based on the "cracking" model has

* Corresponding author. Tel.: +1 217 333 6291; fax: +1 217 333 1750.
E-mail address: shin5@illinois.edu (H. Shin).

0167-9317/$ - see front matter © 2008 Elsevier B.V. All rights reserved.
doi:10.1016/j.mee.2008.10.009

already been investigated by others using synchrotron beam lines [11–13], electron beam [14,15], and even EUV light exposure [8]. Furthermore, a comprehensive model of carbon contamination [16] has been developed by combining the previous hydrocarbon cracking model [11] with the transport of residual hydrocarbons to the irradiated area. In this study, however, we will take into account the effect of energetic ion sputtering in the EUV source environment. This study will represent what is predicted by other models [11,16] or observed experimentally [8,11–16] with a different point of view. In particular, our model will explain the faster carbon growth rate with cracking by sputtering in conjunction with photoelectron emission on the surface in the beginning of carbon deposition. The results of this study show that the life time of EUV mirrors may be shorter than what is predicted in other laboratory EUV source systems [17,18] due to continued hydrocarbon cracking by energetic ions.

2. Experiment

Fig. 1 shows the experimental setup used in this reflectivity degradation experiment. The EUV light source used for this study was the XTREME technologies XTS 13-35 DPP source. This source generates a z-pinch plasma hot ($T_e \sim 30$ eV) enough to emit EUV photons. An experimental chamber has been connected to the XTS 13-35 source flange in order to provide a means to introduce diagnostics into the EUV system. A more detailed description of the system can be found in other previously published literatures [19,20]. In this investigation, Xe was used as a fuel for EUV light production. The system used one Osaka TG-M series turbo molecular pump, backed by an Ebara Model 80X25 UERRGM blower and two Welch belt-driven pumps in order to evacuate the chamber. With this pumping system, the main chamber base pressure could be kept in the low 10^{-6} Torr. An SRS-100 residual gas analyzer (RGA) was used at one of the ports available on the chamber to monitor water vapor pressure.

In this experiment, four samples were placed in XTS 13-35 EUV source chamber at 23° grazing incidence angle with respect to the pinch location. The samples used for this study were 100 nm Ru capped Si wafer prepared by ion beam sputtering. The original rms (root-mean-square) roughness of each sample was 0.6 nm. There are four sample locations within the chamber, with each having a mounting port, load-lock extraction port, viewing window, and thermocouple feed through for temperature measurement. Each sample holder is equidistant from the *z* axis. Fig. 2 shows a schematic of sample manipulation by the load-lock. The load-lock apparatus allowed samples to be removed during tests at varying exposure durations without disturbing the remaining samples. This is critical to minimize transient effects that are caused by electrode thermal cycling from discontinuous source operation. The sample holder apparatus is a custom designed aluminum block with indentations for mirror sample positioning with grazing incidence.

The pinch was operated with 85 sccm of Xe gas in conjunction with a foil trap with 200 sccm of Ar gas. The resulting total flux count of ion debris was measured using ESA system [20] as 9.8 million ions/cm^2-pulse at the location of the samples. Furthermore, the system was baked using halogen lamps before the experiment, achieving 3×10^{-6} Torr total base pressure in order to reduce the amount of excess water present within the chamber. The partial water pressure after baking out was measured as 1×10^{-6} Torr by RGA.

The pinch was operated with a fixed repetition rate of 450 Hz. Each sample was unloaded without disturbing pinch operation. This was done by quickly attaching and detaching the load-lock system to different gate valve after desirable amount of exposure time. The samples were exposed to 0.5, 1, 2.5, and 4 million shots respectively.

After EUV exposure, the roughness of the samples was measured using atomic force microscopy (AFM). Furthermore, Auger electron spectroscopy (AES) was used to measure the contamination on the exposed samples. The surface was scanned in tapping mode over a 2 μm × 2 μm surface. Three different regions were analyzed from each sample. Lastly, the reflectivity of samples was measured after exposure using the EUV relectometry beam

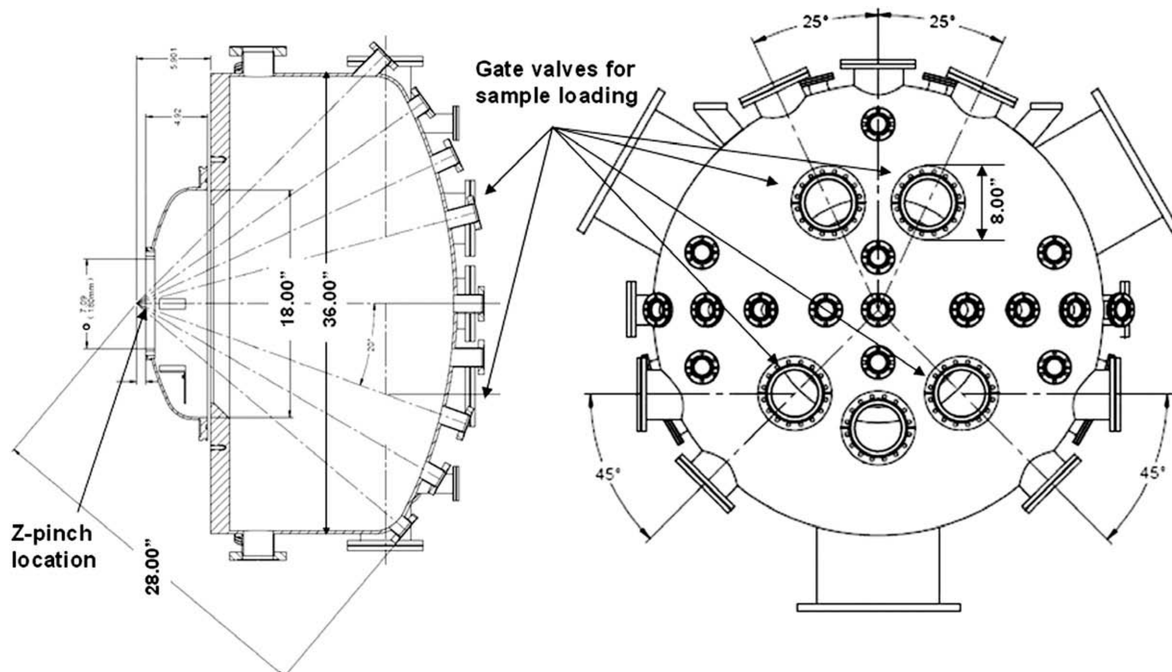

Fig. 1. Schematic of XTS 13-35 used in this study. An experimental chamber connected to the XTS 13-35 source flange providing a means to introduce diagnostics into the EUV system.

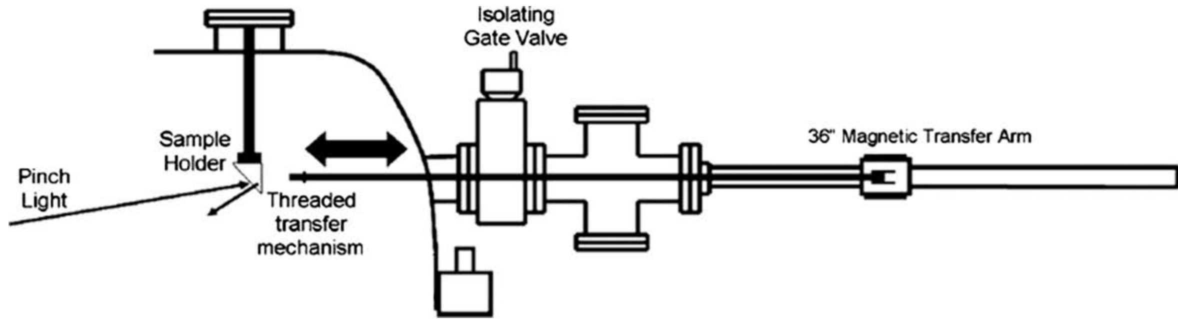

Fig. 2. Schematic of sample transportation system used in this experiment.

line at the Synchrotron Ultraviolet Radiation Facility (SURF III) of NIST (National Institute of Standards and Technology).

3. Results and discussion

3.1. Reflectivity loss by carbon contamination

First of all, the surface roughness change by EUV exposure is summarized in Table 1. The unexposed sample is initially shown to be relatively smooth (0.6 nm of rms roughness). After 0.5 million shot, the surface roughness changed very little but the roughness of the other samples after exposures revealed a slight evolution of roughness of the mirror surface. The highest RMS roughness of 1.4 nm was observed after 4 million shot exposure. The increase of roughness by exposure is due to either erosion by the energetic ions and neutral debris or deposition of contaminants on the samples. The significant increase of maximum height in the scanned area (H_{max}) shows the existence of pits or particles after exposure.

Fig. 3 shows the EUV reflectivity of samples as a function of grazing incidence angle, which were measured by NIST after exposure to the EUV source. The reflectivity of the unexposed sample is also shown together with the predicted reflectivity by CXRO simulator [21] with conditions of 100 nm Ru with rms roughness of 0.6 nm and 2 nm on Si substrate. It is notable that the simulated reflectivity is higher than the measured reflectivity of the original sample. This implies that there is some loss in reflectivity due to means other than surface roughness alone. By the way, the small fall off in the unexposed sample from 5 to 10° is due to the small size of the sample. Another noticeable result is that the measured reflectivity of the other exposed samples was significantly reduced from the unexposed sample. The measured reflectivity is much smaller than prediction even with the roughness of 2 nm, which is somewhat greater than the measured roughness values of exposed samples. Furthermore, in each of the exposed samples, ripples in reflectivity were observed at higher grazing angles; such ripples are likely caused by surface interference properties.

Auger electron spectroscopy (AES) scans of all the exposed samples revealed a strong carbon peak. Although KLL carbon peak (271 eV) is too close to MNN Ru peak (273 eV) to distinguish the two, the presence of C is furthermore supported by the fact that the second strong Ru peak (231 eV) is not observed. [22]. The AES

Table 1
AFM results before and after EUV exposure (Error < 10%).

	RMS (nm)	R_{avg} (nm)	H_{max} (nm)
Unexposed	0.6	0.4	5.8
0.5 million	0.6	0.4	9.0
1 million	1.3	0.6	27.1
2.5 million	1.2	0.9	18.4
4 million	1.4	1.1	11.2

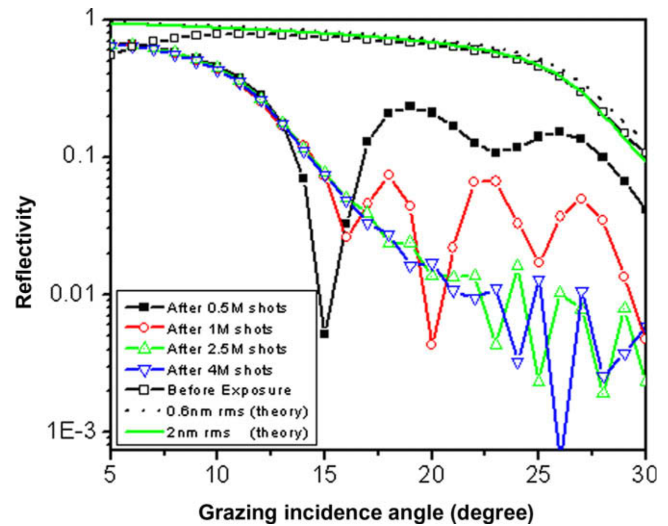

Fig. 3. Results of measured reflectivity at NIST for unexposed, and exposed samples of 0.5, 1, 2.5, 4 million shots along with the simulated reflectivity with 0.6 nm and 2 nm rms roughness.

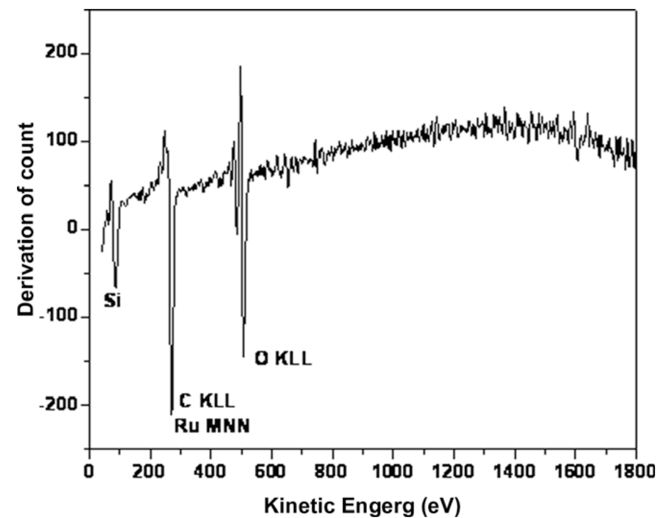

Fig. 4. AES scan result of the sample after 1 million shots exposure.

scan result of the sample after 1 million shots exposure is shown in Fig. 4. This figure shows the overlap of C and Ru peak but no strong second Ru peak. The XTS 13-35 EUV source system used for this study is dedicated to a variety of experimental measurement. Therefore, poor cleanliness of the system can be easily con-

tributed to carbon contamination. Moreover, the carbon tape used for sample mounting is also a significant source of carbon contamination when it is heated, in this case, by ion and photon flux energy transfer [23]. A combination of reflectivity loss with ripples and the presence of carbon on the surface implies that the carbon contamination accumulated on the samples during EUV exposure. Taking this into consideration, the measured data were fitted by changing only the carbon film thickness using a bi-layer mirror model in the CXRO simulator [21]. For simulation, the surface roughness of 2 nm was used although it is somewhat higher than real measurement. In Fig. 3, however, it is already shown that a small change of roughness does not affect the reflectivity to the extent seen.

The measured reflectivity of each sample along different grazing incidence angle is shown with the fitted reflectivity by the carbon deposition thickness in Fig. 5. The uncertainty in the measurement of absolute reflectivity at the Synchrotron Ultraviolet Radiation Facility (SURF III), NIST is 0.35%. The fitted reflectivity with the carbon contamination shows a reasonably good agreement with the measured data overall. For the case of 0.5 million shots, the measured data are fitted better with smaller density d' (1.367 g/cm^{-3}) than normal density value d (2.267 g/cm^{-3}). This implies that the thin film is not as dense as solid carbon when carbon deposit is thin. The reason is that photoelectrons from the bottom Ru mirror surface will crack carbon bonds and, accordingly, lower the density. For other cases, the measured data and the simulated values match reasonably well with the normal density value of carbon. The small discrepancy can originate from the change of absorption coefficient by oxidation or impurities.

The carbon contamination thickness along exposure time deduced from the results of Fig. 5 can be seen in Fig. 6. As exposure time increases, the thickness of carbon film on Ru mirror increases. This clearly shows that the carbon contamination is proportional to exposure time. In Fig. 6, it is notable that the contamination rate appears faster in the beginning of contamination. The dashed line in Fig. 6 is there to guide an eye indicating faster contamination rate when carbon buildup starts even though we do not have measured data below 35 nm in this investigation. It is observed that contamination thickness increases quite linearly along with the number of shots after 0.5 million shot. This implies that the contamination rate becomes constant after around 30 nm carbon builds up on the surface. From the bare Ru surface, the carbon film starts to grow fast with a rate greater than 7×10^{-5} nm/shot and the growth slows down to 2.2×10^{-5} nm/shot as carbon film builds up. This trend of carbon growth rate change agrees with Boller. Boller et al. explained why carbon growth on Au surface decreases as carbon contamination gets thicker by a photoelectron yield theory [11]. In the same way, as the carbon layer gets thicker, the photoelectrons from Ru surface cannot reach and crack the hydrocarbons on the top surface. Therefore, the contamination rate finally saturates. In addition to this theory, we investigate the fast

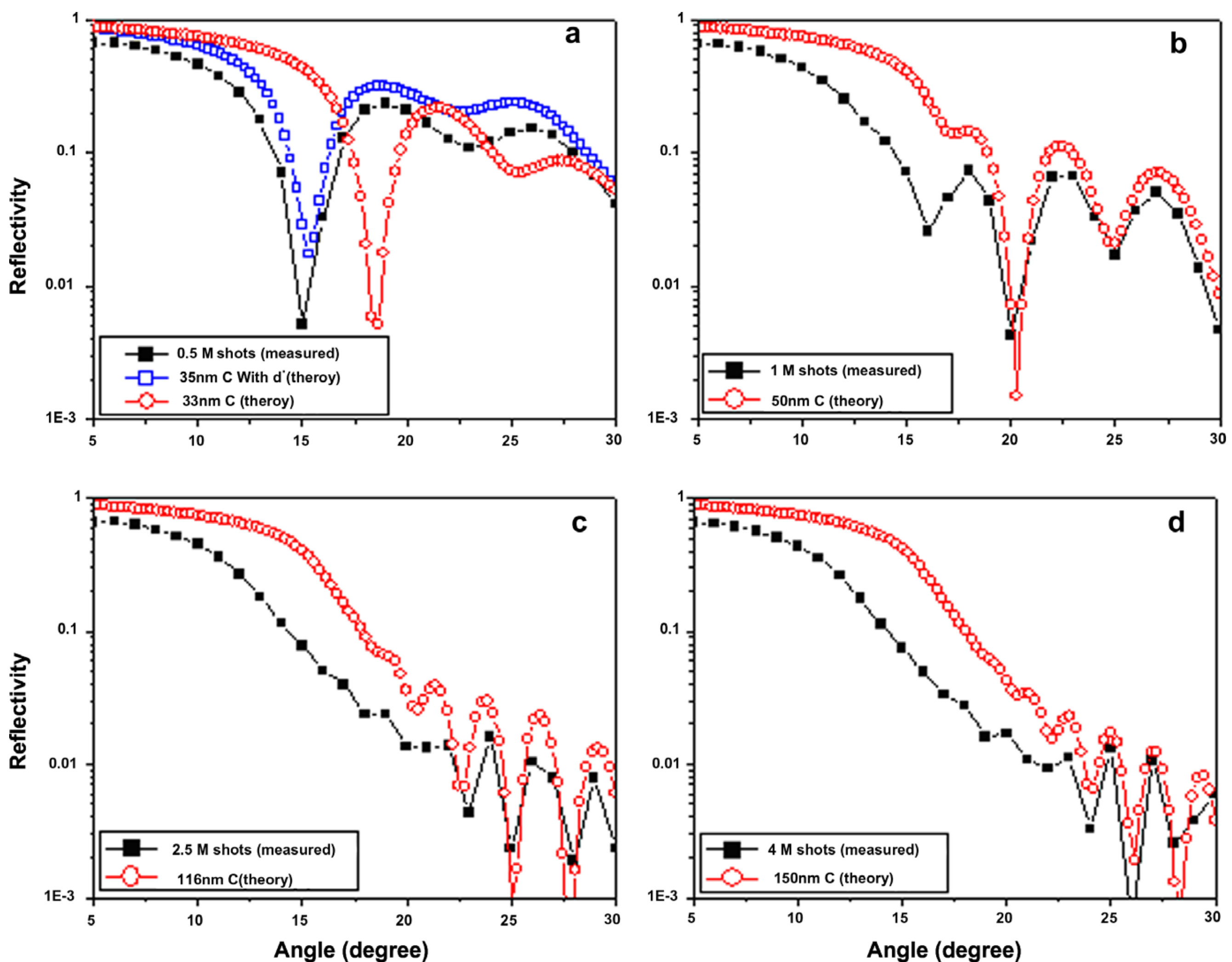

Fig. 5. Experimental (■) and theoretically fitted (○) data using the CXRO simulator for the samples exposed to (a) 0.5, (b) 1, (c) 2.5 and (d) 4 million shots.

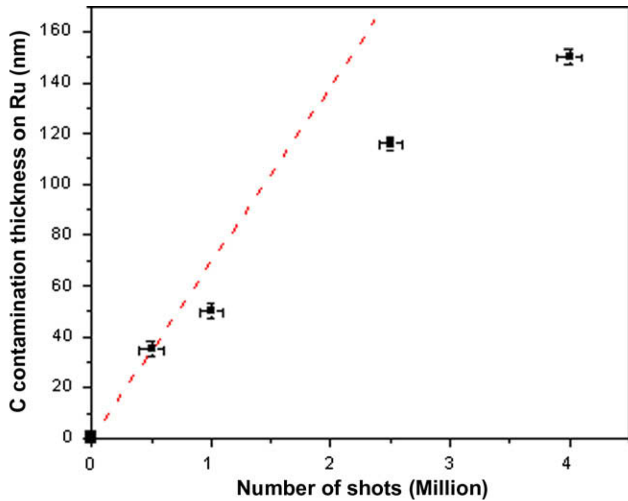

Fig. 6. Thickness of carbon contamination as a function of the number of shots.

growth in the beginning further with sputtering taken into account.

Fig. 7 shows the simulated results of sputtering by energetic Xe ions using TRIM code [24] with 23° grazing incidence angle. The carbon sputtering yield and total sputtering yield (Y_C and Y_{total}) by Xe ions with different energy are plotted in the same graph. When carbon thickness on top of Ru is 1 Å, the carbon sputtering rate is very low since there is a little carbon on the surface. When carbon layer is thin, Ru is also hit by incident Xe ions or carbon atoms and therefore sputtered as well. As carbon thickness on top of Ru gets thicker up to 5 Å, carbon sputtering yield is enhanced because the amount of carbon on Ru increases, whereas Ru sputtering yield decreases. When carbon thickness is greater than 5 Å (carbon is filled in the first few layers underneath the surface), however, carbon is sputtered less than when the heavy atoms (Ru) are underneath the surface. The light carbon atom will keep more energy when it hits heavier atoms than the same weight atoms. Then, sputtering rate reaches the solid carbon sputtering yield results in no Ru sputtering at all as thickness of carbon is thicker than 30 Å.

From the above discussions, the phenomena of carbon build up can be explained as four phases based on the sputtering yield

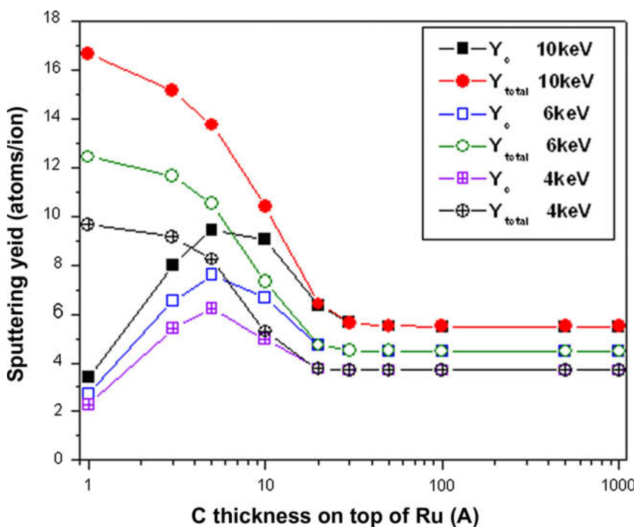

Fig. 7. Sputtering yield vs. carbon thickness on Ru at different energy of incident Xe ions. Y_c is the carbon sputtering yield and Y_{total} is the sum of both carbon and ruthenium sputtering yield simulated by TRIM.

change and density change. In the first phase when carbon thickness is 0 to 2 Å, sputtering is very low but cracking by photoelectron from Ru surface is very high. Therefore, carbon growth rate is very rapid. In the second phase when carbon thickness is 2 to 30 Å, cracking by photoelectron is still high and carbon sputtering is enhanced. This implies that carbon bond breaking by ion sputtering is also occurring. Therefore, overall carbon growth is rapid. In the third phase when carbon thickness is 30 to 300 Å, cracking by photoelectron is still high since the density of the film is lower than the tightly bonded carbon. On the other hand, sputtering rate has reached a steady-state rate giving a constant removal flux by sputtering. Some ion-induced cracking is also going on but with a lower steady state value. So, growth is not as rapid as the previous phases. For the last phase, cracking by photoelectron decreases since photoelectrons are no longer produced as much and cannot reach the surface and crack any carbon compounds. Therefore, growth is slow down and sputtering and photon- and ion-induced cracking are the only mechanisms at work. The photon- and ion-induced cracking is a bit faster than the removal effect from sputtering. Therefore the growth is the slowest in the steady state.

3.2. Carbon contamination rate model

Our model starts from the assumption that hydrocarbons (C_xH_y) only adsorb onto a carbon surface which is not already covered by hydrocarbons. By cracking these hydrocarbons, carbon will be added onto the surface. In an EUV collector, the hydrocarbons can be cracked by energetic ions, EUV photons, or photoelectrons emitted from the Ru surface. From this assumption, the rate of coverage of hydrocarbons can be modeled as follows:

$$\frac{d\theta}{dt} = S(1-\theta)\Gamma_{C_xH_y} - C_1\theta Y T_i - C_2\theta T e^{\Delta E/KT} - C_3\theta I \quad (1)$$

θ is the fraction of hydrocarbon molecules present on the surface and therefore $1-\theta$ is the fraction of cracked hydrocarbon molecules leading to the next carbon layer being formed. $S(1-\theta)\Gamma_{C_xH_y}$ is the generation of new hydrocarbon molecules by adsorption on the carbon layer with sticking coefficient S. $\Gamma_{C_xH_y}$ is the incoming hydrocarbon flux onto the surface. In an EUV source system, energetic ions from hot plasma are also present. The term of $C_1\theta Y\Gamma_i$ shows that sputtering by these energetic ions will crack the hydrocarbon molecules so as to lead to formation of the carbon layer. Γ_i is the incoming ion flux onto the surface and Y is the sputtering yield. C_1 is larger than unity since cracking can occur without sputtering. On the surface, there will be a thermal desorption of the hydrocarbon molecules, $C_2\theta Te^{-\Delta E/KT}$. Lastly, $C_3\theta I$ simply shows the cracking of the hydrocarbon molecules by photons and photoelectrons. I is the flux of photons and photoelectrons able to cause cracking.

For the steady state, the fraction of crackable hydrocarbon molecules, θ can be derived as

$$\theta = \frac{S\Gamma_{C_xH_y}}{S\Gamma_{C_xH_y} + C_1 Y\Gamma_i + C_2 Te^{-\Delta E/KT} + C_3 I} \quad (2)$$

The contamination rate by carbon can be assumed linearly proportional to $(1-\theta)$ since carbon builds up from the cracked hydrocarbons. Using Eq. (2), therefore, the rate can be derived as

$$R(t) = k\frac{1}{1 + \frac{S\Gamma_{C_xH_y}}{C_1 Y(t)\Gamma_i + C_2 Te^{-\Delta E/KT} + C_3 I(t)}} \quad (3)$$

Here, k is a proportional constant that correlates the cracked hydrocarbons to the contamination rate. The sputtering yield is varied as the carbon thickness changes on the surface as shown in Fig. 7. Also, the flux I decreases as the thickness grows since photoelectrons from the Ru will no longer be able to reach the surface. Therefore, they are written as $Y(t)$ and $I(t)$ whereas the other terms

are assumed as constants in Eq. (3). $Y(t)$ and $I(t)$ will attain a steady value after the carbon layer grows beyond a certain thickness. Accordingly the contamination rate will eventually arrive at a steady state. The initial contamination rate is predicted to be faster by this model when the carbon layer is thin before $Y(t)$ and $I(t)$ have reached their steady state values as shown below. Assuming the thermal desorption of the crackable molecules is ignorable compared to desorption by ions, photons, and photoelectrons, Eq. (3) can be rewritten as follows:

$$R(t) = \frac{k}{1 + \frac{1}{\frac{C_1 \Gamma_i Y(t)}{S\Gamma_{C_X H_Y}} + \frac{C_3 I(t)}{S\Gamma_{C_X H_Y}}}} \quad (4)$$

C_1 is assumed to be 1.3; S is assumed to be 1. Ion flux, Γ_i is measured by ESA as 5.73×10^9 ions/cm^2 s at a 450 Hz of pinch repetition rate, 0.5 m distance from the pinch. Assuming hydrocarbon molecules are mainly methane (CH_4) and its partial pressure is 0.1% of the processing pressure (1 mTorr), $\Gamma_{CH_4} = (1/4)nv = 1/4 \cdot (3.29\text{x}10^{16} \times \text{P(Torr)}) \cdot (8kT/\pi m)^{1/2} = 5 \times 10^{17}$ molecules/cm^2 s [25], where n is molecule density at given pressure and v is the thermal velocity based on Maxwellian distribution.

A reasonable value of $I(t)$ is found by assuming $I(t) = (1+Y_{PE}(t))\Phi$, where Φ is the EUV photon flux from z-pinch in our experiment, which can be estimated from photodiode measurement in our system. Given EUV photons are collimated through 1 mm^2 pinhole and hitting a photodiode through a EUV (13.5 nm) tuned multilayer mirror with 65% reflectivity, the total charge Q measure by an oscilloscope can be converted into photon flux. Using known quantum efficiency (QE) of the photodiode ($\sim$1), the total charge density generated by the photodiode can be calculated as 2×10^{-12} C/mm^2 during one pulse. This leads to the photon flux as 2×10^{-12} C/mm^2 $\times$ 1 photon/1 electron/(1.6×10^{-19} C), that is 1.25×10^9 photons/cm^2 onto the photodiode. This corresponds to 8.65×10^{11} photons/cm^2 sec incoming from the pinch. $Y_{PE}(t)$ is the number of photoelectron emitted from Ru surface by an incoming EUV photon and successfully reaching to the top surface, which varies along time since contamination thickness grows as time elapses. The simplest estimation for $I(t)$ is then that it exponentially decrease from the maximum $(1+Y_{PE}(0))\Phi$ to minimum Φ. Our best estimation for $Y_{PE}(0)$ is 1 by using a photoelectron yield of gold at a similar photon energy (at 100 eV) [26] and taking into account that photoelectron yield is affected by temperature [11].

With these values and assumptions, the contamination rate predicted by Eq. (4) is shown in Fig. 8 with C_3 equal to 0.16 and k equal to 11[nm/shot]. This figure shows the change of contamination rates along with the elapsed number of shots. The contamination rate starts fast and then reaches a steady state. The measured contamination rate from Fig. 6 is overlayed on the model. The fit is what determines C_3 and k. Some discrepancy may be due to ignoring thermal desorption in our model and the calculation of the contamination rate by using pairwise slopes from Fig. 6 rather than taking the derivative of a continuous contamination thickness change vs. time.

Fig. 9 shows the estimated photon and photoelectron flux as a function of time. Given the photon flux from EUV source, the change of photoelectron flux escaping from the carbon layer accounts for the decay of $I(t)$. $I(t)$ becomes stable around 0.1 million shots. From our measurement at 0.5 million shot, the thickness of carbon layer on Ru is estimated as several nanometer. This is in agreement with previous observation by other researchers. They observed a transition from fast to slow contamination around 5 nm [11].

The significance of Fig. 8 and Fig. 9 can be summarized as twofold. One is that the faster contamination rate is caused by varying sputtering yield and photoelectron intensity in the early stage of contamination. The other is that contamination reaches steady

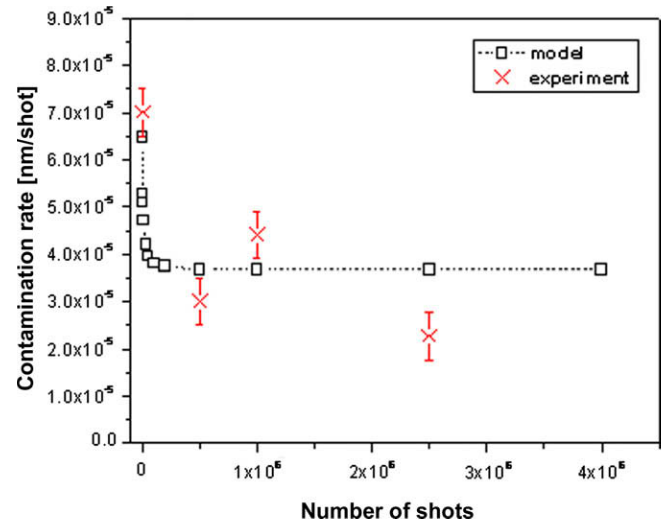

Fig. 8. Comparison of the carbon contamination rates derived by experiment and predicted by the model developed in this study.

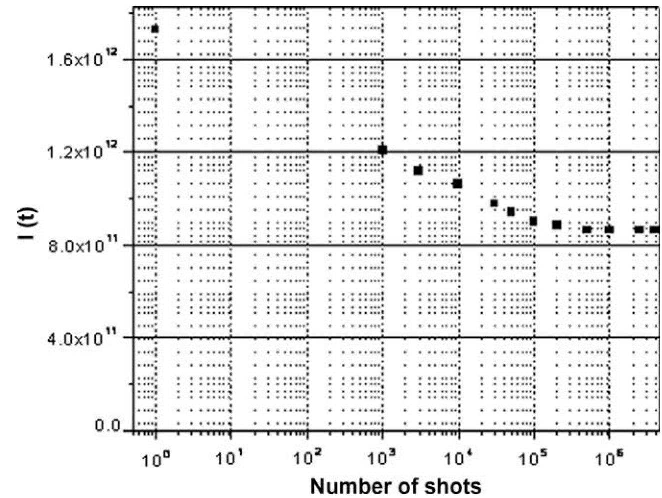

Fig. 9. The estimated photon and photoelectron flux as a function of number of shots.

state after a certain thickness of carbon builds up and contamination continues. However, this steady state rate will be higher than what is predicted by only photons and photoelectrons since there are also energetic ions to crack hydrocarbons by sputtering on EUV collector optic systems.

4. Conclusion

In this study, the effect of EUV exposure time on EUV mirrors was investigated. Four samples were placed in the XTS 13-35 EUV DPP source and each sample was retrieved after certain exposure time. In the system under this investigation, all the samples showed carbon contamination buildup and, accordingly, reflectivity degradation when measured by the NIST EUV beam line. The results show that carbon buildup rate changes with exposure time and carbon buildup. In the beginning of contamination, the contamination rate is fast as 7×10^{-5} nm/shot, but diminishes down to 2×10^{-5} nm/shot as contamination proceeds. These differing contamination rates are explained by the change in sputtering yield of the contaminated mirror surface in conjunction with carbon contamination thickness allowing Ru photoelectrons to

interact with the surface. The findings in this study will help to understand fast initial carbon contamination and will aid in improving lifetime of EUV mirrors by minimizing contamination due to EUV exposure and carbon contamination. Since energetic ion sputtering is found to be responsible for continued contamination, it is critical for longer lifetime to reduce energetic ion flux to EUV mirror surfaces.

Acknowledgements

We would like to express our thanks to Frank Goodwin from SEMATECH for his kind support and funding from SEMATECH. We are thankful to Intel for partially funding this research. We would like to sincerely thank Dr. Steven Grantham in NIST for reflectivity measurement. The sample analysis was carried out in part in the Frederick Seitz Materials Research Laboratory Central Facilities, University of Illinois, which are partially supported by the U.S. Department of Energy under Grants DE-FG02-07ER46453 and DE-FG02-07ER46471. We would also like to thank the Center for Microanalysis of Materials, University of Illinois for the help of sample analysis.

References

[1] J.P. Allain, M. Nieto, A. Hassanein, Appl. Phys. A 91 (2008) 13–16.
[2] J.P. Allain, M. Nieto, M. Hendricks, A. Hassanein, C. Tarrio, S. Grantham, V. Bakshi, Proc. of SPIE 6517 (2007) 65171V-1.
[3] M. Nieto, J.P. Allain, V. Titov, M.R. Hendricks, A. Hassanein, D. Rokusek, C. Chrobak, J. Appl. Phys. 100 (2006) 053510.
[4] A. Barty, K.A. Goldberg, Proc. of SPIE 5037 (2003) 450–459.
[5] M.L. Scott, P.N. Arendt, B.J. Cameron, J.M. Saber, B.E. Newnam, Appl. Optics 27 (8) (1988) 1503.
[6] D.J.W. Klundera, M.M.J.W. van Herpen, V.Y. Banine, K. Gielissen, Proc. of SPIE 5751 (2005) 943.
[7] H. Shin, S.N. Srivastava, D.N. Ruzic, J. Vac. Sci. Technol. A 26 (3) (2008) 389–398.
[8] M. Malinowski, P. Grunow, C. Steinhaus, M. Clift, L. Kiebanoff, Proc. of SPIE 4343 (2001) 347.
[9] L.E. Klebanoff, M.E. Malinowski, W.M. Clift, C. Steinhaus, P. Grunow, J. Vac. Sci. Technol. A 22 (2) (2004) 425.
[10] D.J. Davis, G. Kyriakou, R.B. Grant, M.S. Tikhov, R.M. Lambert, J. Phys. Chem. C 111 (33) (2007) 12165.
[11] K. Boller, R.-P. Haelbich, H. Hogrefe, W. Jark, C. Kunz, Nucl. Instrum. Methods 208 (1983) 273.
[12] R.A. Rosenberg, D.C. Mancini, Nucl Instrum Methods A 291 (1990) 101–106.
[13] M. Niibe, Y. Kakutani, K. Kakichi, S. Terashima, H. Takase, Y. Gomei, T. Aoki, S. Matsunari, H. Kondo, Y. Fukuda, Jpn. J. Appl. Phys. 44 (7B) (2005) 5552–5555.
[14] N. Koster, B. Mertens, R. Jansen, A.V. Runstraat, F. Stietz, M. Wedowski, H. Meiling, R. Klein, A. Gottwald, F. Scholze, M. Visser, R. Kurt, P. Zalm, Microelectron. Eng. 61–62 (2002) 65–76.
[15] R. Kurt, M.V. Beek, C. Crombeen, P. Zalm, Y. Tamminga, Proc. of SPIE 4688 (2002) 702.
[16] H. Meiling, H. Meijer, V. Banine, R. Moors, R. Groeneveld, H.J. Voorma, U. Mickan, B. Wolschrijn, B. Mertens, G. van Baars, P. Kürz, N. Harned, Proc. of SPIE 6151 (2006) 615108.
[17] B. Mertens, M. Weiss, H. Meiling, R. Klein, E. Louis, R. Kurt, M. Wedowski, H. Trenkler, B. Wolschrijn, R. Jansen, A.V. Runstraat, R.M. Karel Spee, S. Plöger, R.V. Kruijs, Microelectro. Eng. 73-74 (2004) 16–22.
[18] J. Hollensheada, L. Klebanoff, J. Vac. Sci. Technol. B 24 (1) (2006) 64.
[19] XTREME Technologies GmbH, Gottingen, Germany <www.xtremetec.de>.
[20] K.C. Thompson, E.L. Antonsen, M.R. Hendricks, B.E. Jurczyk, M. Williams, D.N. Ruzic, Microelectron. Eng. 83 (2006) 476–484.
[21] Deduced from a simulation tool of X-ray interactions with Matter, Center for X-ray Optics <www.cxro.msd.lbl.gov/>.
[22] L.E. Davis, N.C. MacDonald, P.W. Palmberg, G.E. Rich, RE Weber, Handbook of Auger Electron Spectroscopy, second ed., Physical Electronics Division Perkin–Elmer Corporation, Eden Prairie, MN, 1978.
[23] R. Garg, A. Wüest, E. Gullikson, S. Bajt, G. Denbeaux, Proc. of SPIE 6921 (2008) 692136-1.
[24] J.F. Ziegler, SRIM & TRIM, <www.srim.org/index.htm>.
[25] D.N. Ruzic, Electric Probes for Low Temperature Plasmas, AVS, New York, 1994 (Chapter 1).
[26] B.L. Henke, J.P. Knauer, K. Premaratne, J. Appl. Phys. 52 (3) (1981) 1509–1521.